Herschel - SPIRE: Optical Error Budgets

SPIRE-LAM-PRJ-000446

RAL	K.King			
	B.Swinyard	X		
CNES	M.Joubert		Y.Blanc	
CEA-Sap	Jean-Louis Auguères			
LAS	J.P.Baluteau	X	D. Ferrand	
	K.Dohlen	X	R. Malina	
	A.Origné	X	P.Dargent	X
	D.Pouliquen	X		

LABORATOIRE D'ASTROPHYSIQUE DE MARSEILLE - CNRS BP 8 13376 MARSEILLE Cedex 12 FRANCE
Tél : (33) +4 91 05 59 00 - Fax : (33) +4 91 05 69 59

Updates

Date	Indice	Remarks
22 May 2000	DRAFT	Creation of the document
30 June 2000	1	First release
5 December 2000	2	Exact sized photometer cold stop. Focus budget
22 August 2001	3	Telescope name changed. Baseline systems updated. Telescope and focus added to wavefront budgets. Telescope alignment included in Phot pupil alignment budget. Pupil alignment added in Spec throughput budget. Fringe contrast calculations revised for clipped Gaussian.

Reference documents

#	Title	Author(s)	Reference	Date
1	FIRST alignment plan		PT-PL-02220	9/5/96
2	“Martin-Puplett interferometer: an analysis”	Lambert, Richards	Applied Optics **17**, 1595 (1978)	1978
3	Filters, Beam Splitters & Dichroics	P.A.R. Ade, C.E Tucker M.J. Griffin, P.C.Hargrave	SPIRE Preliminary Design Review	7-9 July 1999
4	"The calculation of image quality", p.225	W. B. Wetherell	Appl. Opt. and Opt. Eng., vol VIII, Eds R. R. Shannon, J. C. Wyant, Academic Press, London	1980

Host system	Windows NT
Word processor	Microsoft Word 97
File	ErrorBudgetsV3_02.DOC
Printed	30/10/01 11:05

1. Scope

This document presents optical error budgets for SPIRE.

1.1. Table of contents

2. Introduction

Optical error budgets for the SPIRE instruments are presented. Throughput and wavefront error (Strehl ratio) budgets are presented for both photometer and spectrometer channels. Alignment tolerances are considered by way of a pupil alignment budget for the photometer and an interferogram contrast budget for the spectrometer.

2.1. Baseline designs

Current baselines are BOLPHT155 for the photometer channel and BOLSP502 for the spectrometer channel. Schematic representations of the systems with symbolic names for each component are shown in Figure 1.

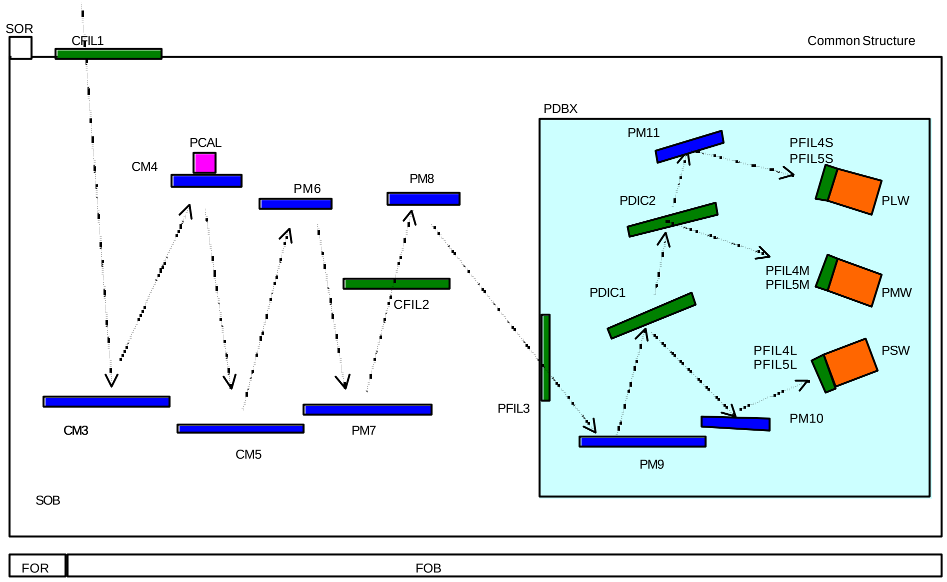

(a)

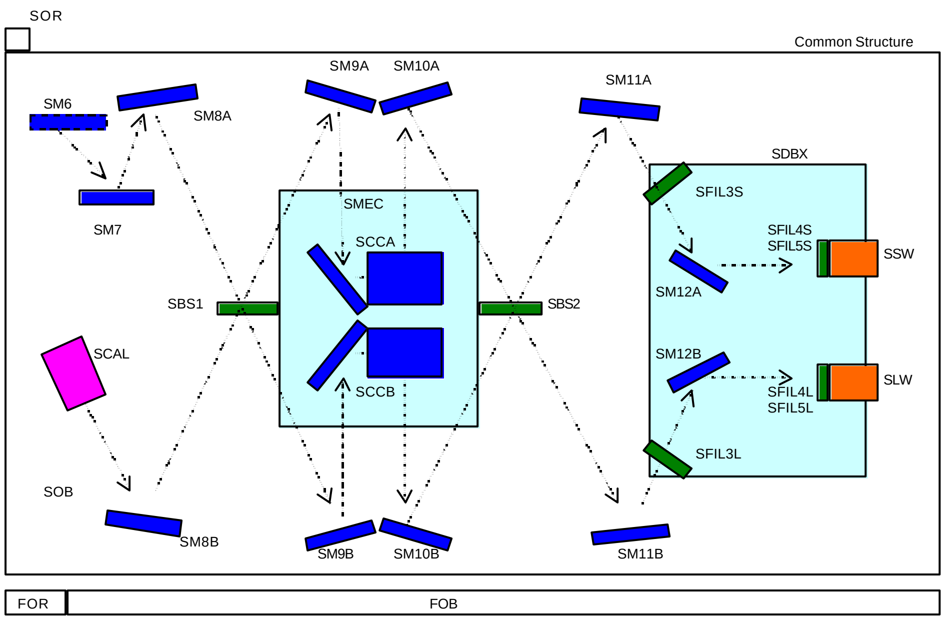

(b)

Figure 1. Schematic layout of the photometer channel (a) and spectrometer channel (b) of the SPIRE instrument.

3. Photometer budgets

3.1. Throughput

Apart from filters and dichroics, major part of budget is due to sizing of cold stop. Undersizing was originally assumed, but it has been proven acceptable to use exact sizing of the cold stop. This means that the cold stop within the SPIRE instrument is given the dimensions of the geometrical image of the telescope pupil (M2). Due to variations in the pupil image for different points in the FOV (pupil aberrations) and instrument misalignments (see alignment budget, Sec. 3.3), the cold stop will not be exactly aligned with the telescope pupil, however, resulting in a loss of throughput. This loss has been estimated by considering the common area of displaced circles, see Figure below.

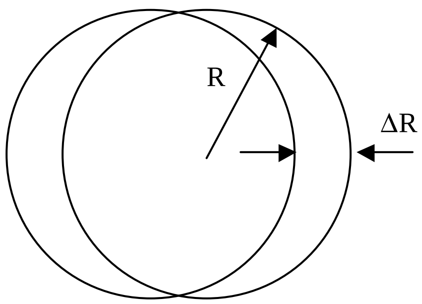

The transmission of the resulting system equals the fraction of the overlapping area (A) to the pupil area (A_0). With analogy to the calculation of optical MTF (see sec. 4.3.2), this fraction may be given by the approximation:

$$\frac{A}{A_0} \approx 1 - \frac{4}{p}u = 1 - \frac{2\Delta R}{pR} = 1 - 0.64\frac{\Delta R}{R}.$$

where $\Delta R/R$ is the fractional displacement between the two circles.

Diffraction and baffling losses have been estimated to 20% (TBC). Reflection efficiency assume a reflectivity of 99% per surface for 8 mirror surfaces. Total filter and dichroic transmission has been assumed to be within the specified 40%.

Horn coupling efficiency is not included.

Current throughput budget (see Fig 2) is in accordance with the IRD requirement.

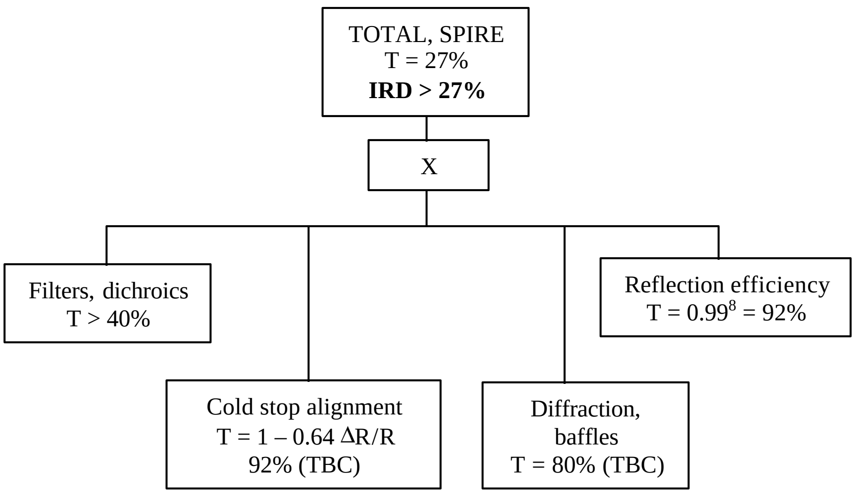

Figure 2. Photometer throughput budget.

3.2. Wavefront error

Figure 3 shows the budget of root mean square wavefront errors (WFErms) for the SPIRE photometer including telescope. It is divided into three main parts: SPIRE instrument, the telescope system, and external alignments. Astrium is responsible for both telescope and external alignment, but the error budget provided by Astrium France (Matra) for the telescope (view graphs from Working meeting at ESTEC 19 June 2001) does not appear to include the alignments between the telescope sub-system and the instruments. To our knowledge, no budget has been provided for this alignment, but as can be seen, assuming three alignment stages each with 1 mm error, this does not add significantly to the budget, even when algebraic summing is used. The resulting 3 mm defocus corresponds to only 1.4 µm wavefront error (see 3.2.1 below).

Unless otherwise noted, the budget is obtained by RSS summing of individual contributions:

$$WFErms^2 = \sum_i WFErms_i{}^2$$

Focus errors and higher order aberrations are treated equally. Since the IRD requirement is given in terms of Strehl ratio, all wavefront errors are accompanied by their Strehl ratio equivalent calculated by the Marechal approximation at $\lambda = 250$ µm:

$$S \approx 1 - \frac{4p^2}{l^2} WFErms^2$$

3.2.1. Defocus contributions

Wavefront error due to defocus Δz is given by:

$$WFErms = \frac{\Delta z}{16\sqrt{3}F^2}$$

At the telescope focus, with F = 8.68, this becomes *WFErms* [µm] = 0.48 Δz [mm]. At the instrument focus, with F = 5, we have *WFErms* [µm] = 1.44 Δz [mm]. None of the defocus contributions assumed in the budget are significant.

3.2.2. Mirror fabrication

The mirror fabrication budget has been separated into two parts, considering surface shape and radius of curvature separately. A specification on radius of curvature of $\Delta R/R = 10^{-3}$ has been assumed for each surface. This may be translated into a wavefront error contribution per surface of

$$WFErms = \frac{h^2}{2\sqrt{3}\,R}\frac{\Delta R}{R}$$

where *h* is sub-pupil radius at the surface and *R* is nominal radius of curvature. Table 1 shows results of these calculations for each surface in the photometer optical train.

A WFErms of 2 µm per reflecting surface (ie, 1 µm rms measured on the surface itself) has been assumed for each of 9 surfaces (CM3 to PM9 plus 1 dicroic plus 1 fold mirror). The total budget entry is: WFErms = $\sqrt{9}$ x 2 µm = 6 µm.

No contribution is assumed for transmissive components (filters and dichroics) since they are assumed to have zero optical thickness.

3.2.3. Internal alignment

Internal alignment has been given very strict tolerances in order to ensure pupil alignment, as described in Sec. 3.3. The effect of alignment errors on the wavefront budget is therefore negligible. Additional allocations of 0.5 mm in axial alignment of detectors with respect to the instrument focal plane and the instrument with respect to the telescope focal plane have been given, but these are seen to be insignificant as well.

The IRD requirement of S > 0.9, corresponding to WFErms < 12.6 µm, is achieved with good margin.

Table 1. Defocus wavefront error due to $\Delta R/R = 10^{-3}$ precision on radius of curvature for each surface

Mirror	R	h	ΔR	WFErms
CM3	370	5.5	0.37	0.02
CM5	300	18	0.3	0.31
PM6	300	0.03	0.3	0.00
PM7	330	19	0.33	0.32
PM8	290	18	0.29	0.32
PM9	350	35	0.35	1.01
Total				1.15

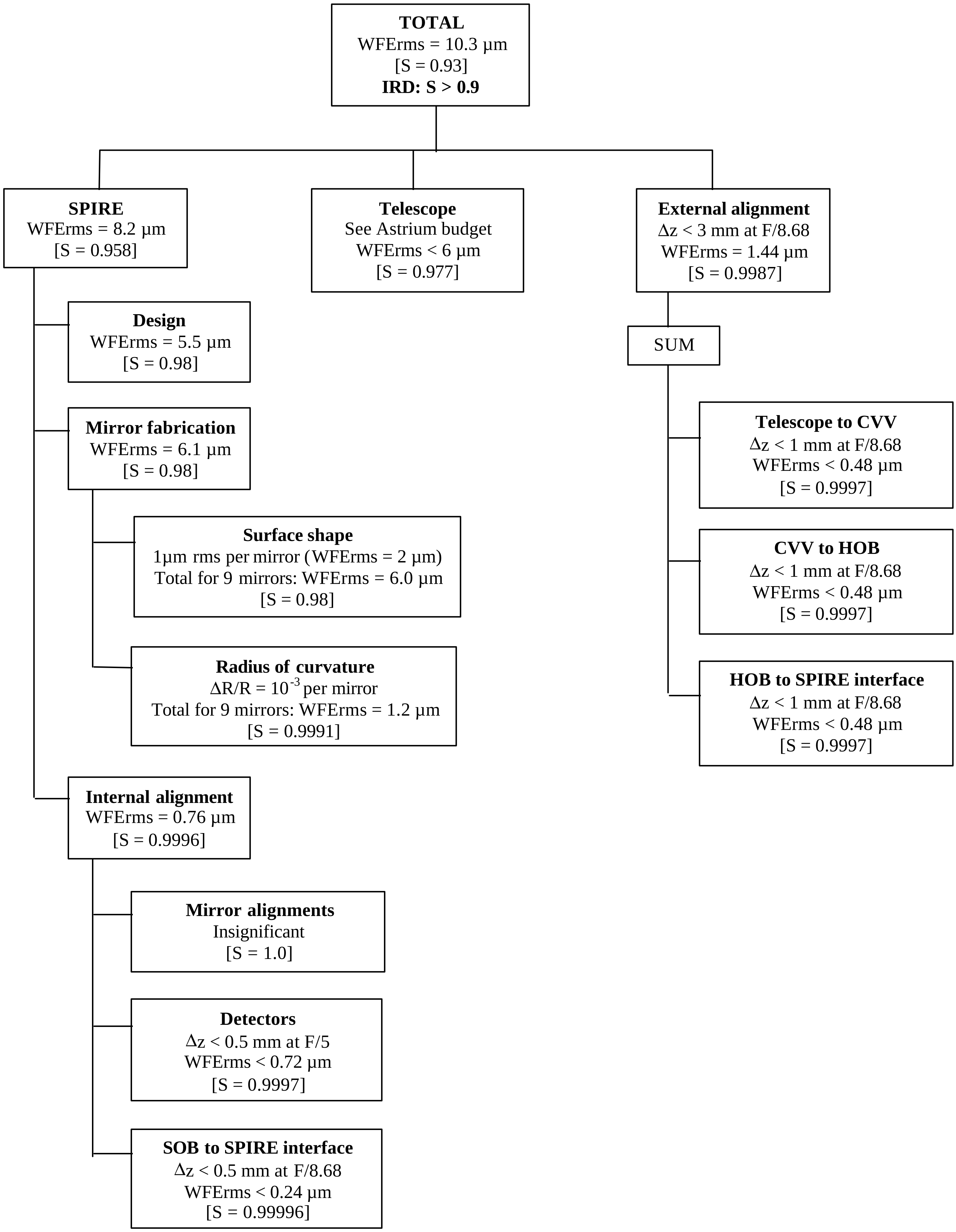

Figure 3. Photometer wavefront error budget.

3.3. Pupil alignment

The pupil alignment budget (Fig. 4) is dimensioning for mechanical tolerances in the photometer case. There is no IRD on pupil alignment, but, as has been shown in the throughput budget (Fig. 2), it has a strong influence on instrument throughput.

The three major components concern design and alignment (Herschel and SPIRE), outlined in heavy lines in the figure. The design value quantifies the variation in pupil position for different points in the FOV for a perfectly aligned instrument, due to pupil aberrations. We believe that this value has been minimized for the optical concept chosen, and that a further reduction would require important complications of the optical design.

Degradation of pupil alignment due to mechanical misalignment consists of errors under ESA control (alignment between the Herschel telescope and its optical bench, HOB) and errors under SPIRE control. These are again broken down to individual error sources.

The budget shows a good balance between its three major components. The contribution from instrument alignment is the smallest, indicating that no great improvement can be expected from reducing the mechanical tolerance values.

3.3.1. Telescope to SPIRE interface

The ESA alignment plan [RD1] provides a total budget for absolute alignment between telescope and instrument of *“12¢ which corresponds to 16 mm lateral misalignment”*. Unfortunately, the document does not provide enough information to translate this into relative pupil alignment ($\Delta R/R$), and using data from the current telescope design (focal ratio F = 8.68, secondary diameter D_{M2} = 308.1 mm), the two quoted numbers give different results. Calculated using the focal ratio and the angular tolerance:

$$\Delta R/R = 2\ F\ \delta\alpha = 6\%,$$

while using the M2 diameter and the linear tolerance:

$$\Delta R/R = 2\ \Delta R/D_{M2} = 10\%.$$

The former is nevertheless assumed for the IID-B specification. This specification has been RSS divided into three parts corresponding to the three etapes of the Herschel integration defined in the presentation by Astrium of 19 June 2001. For each part we have considered two tilt components and two displacement components, i.e. a total of 4 degrees of freedom (DOFs). The resulting requirements (2.6mm decentering and 3.5' tilts) are in line with the analysis performed by T. Richards (Note TBD of 18 July 2001).

3.3.2. Instrument alignment

The instrument alignment budget consists of three parts: SPIRE optical bench (SOB) to instrument interface points (legs), interfaces between SOB and mirrors, and interface between SOB and the cold-stop. Mechanical tolerances have been set to 0.1 mm decenter for each component along each direction x, y, z and 1arcmin tilt for each component around each axis. The effect of misalignments equal to these values for each component and each axis are obtained from a sensitivity analysis, summarized in Figure 5 (BolPhtRev05.mac, SpirePhotTol18.xls). Verification of the effect of random distributions of alignment errors is shown by the histogram plot of Figure 6 (SpirePhotTol20.xls).

Note that the components following the cold stop (PM9, folds, dichroics) have no influence on the CS alignment budget. Also, filters are not included since their thickness, and hence beam deviation, is negligible (TBC PA).

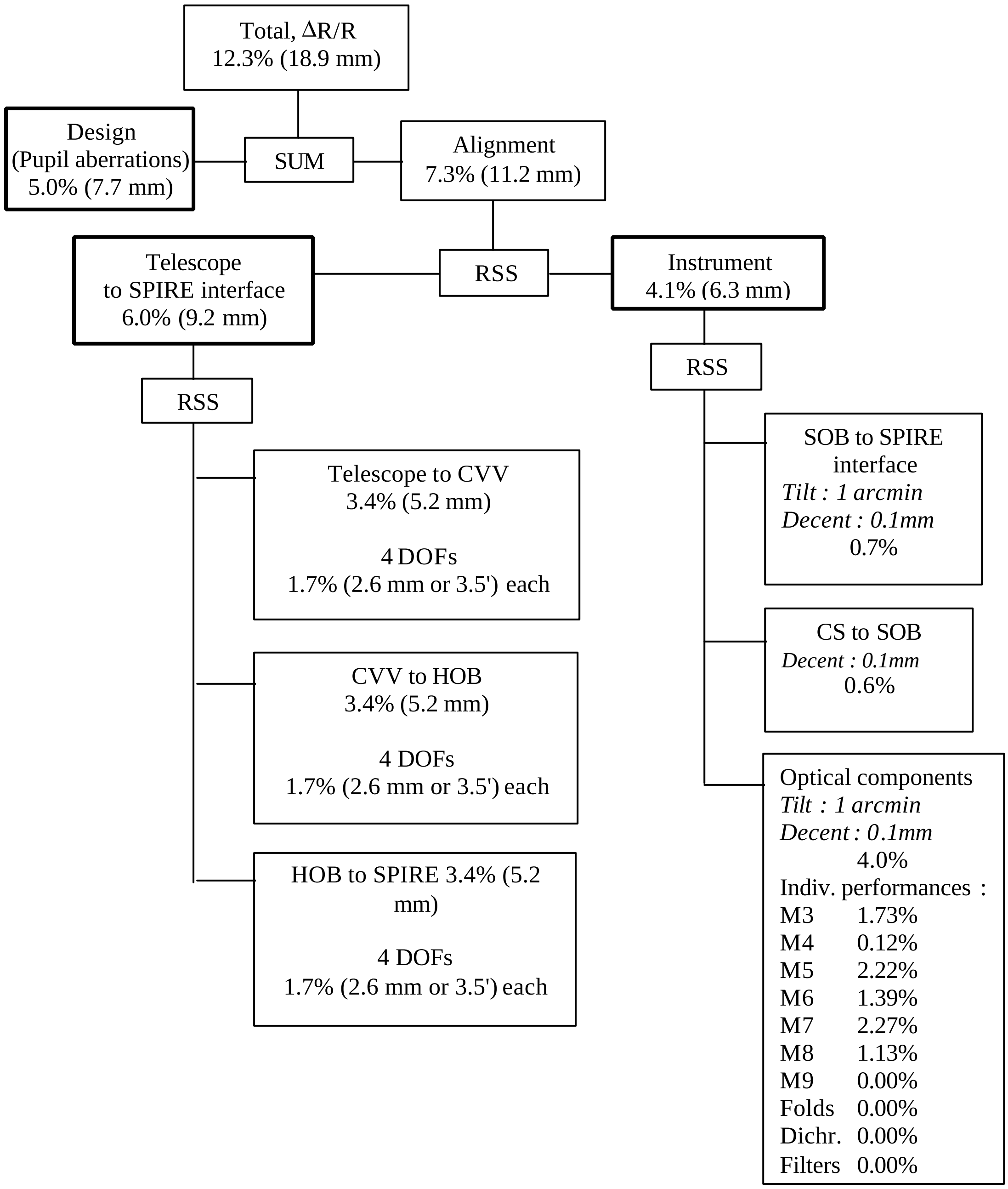

Figure 4. Pupil alignment budget for the photometer. The heavy boxes indicate the tree major components of the budget: optical design (pupil aberrations) telescope alignment under ESA responsibility, and SPIRE alignment.

The SPIRE alignment budget assumes mounting accuracy of 0.1mm and 1arcmin for each interface: the SPIRE optical bench (SOB) mounted on the Herschel optical bench (HOB), each mirror in the optical train mounted on the S-bench, and the cold stop (CS) mounted on the SOB. These tolerances should in each case be distributed on the required intermediate interfaces. For example, the CS is mounted on the 2K box which is in turn mounted on the SOB.

The two top budget components, design and alignment, are summed because the pupil aberrations are deterministic. All other components are "root-sum-squared". As shown by Monte-Carlo simulation (Figure 6 below), assuming a uniform statistical distribution of errors within the tolerance bounds, this budget covers more than 90% percent of the real cases.

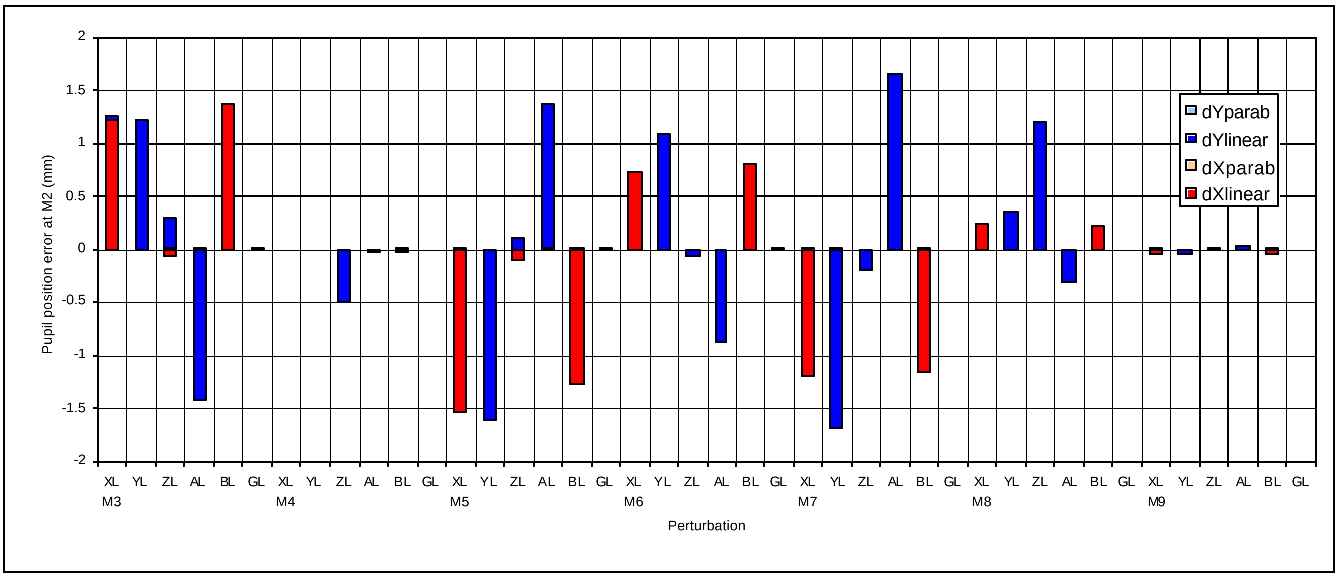

Figure 5. Sensitivity of each photometer mirror to 0.1mm decenter tolerance (XL along x axis, YL along y axis, ZL along z axis) and to 1arcmin rotation tolerance (AL around x axis, BL around y axis, GL around z axis). Apart from M3 and M5, the z axis is perpendicular to each surface at its apex, the y axis is perpendicular to z in the plane of the system, the x axis is perpendicular to y and z. For M3 and M5, the z axis is shifted by 20mm so as to coincide approximately with the centre of gravity of the mirrors, and tilted so as to be perpendicular to the surface at that point.

Results are in mm measured at the M2. For an M2 radius of 150mm, an error DR = 1mm corresponds to a fractional pupil alignment error of DR/R = 0.67%. Red bars show displacements along the x direction, blue bars along the y direction. Light blue and light red correspond to non-linear sensitivity components: these are clearly insignificant.

Apart from M4 (conjugated with the pupil) and M9 (not involved in pupil imaging since after the cold stop), all mirrors have similar sensitivities. Errors due to GL tilts (azimuth rotation) are very small for all mirrors, the alignment budget is not dimensioning for these perturbations. A tolerance of about 0.5 degrees is probably acceptable to avoid vignetting.

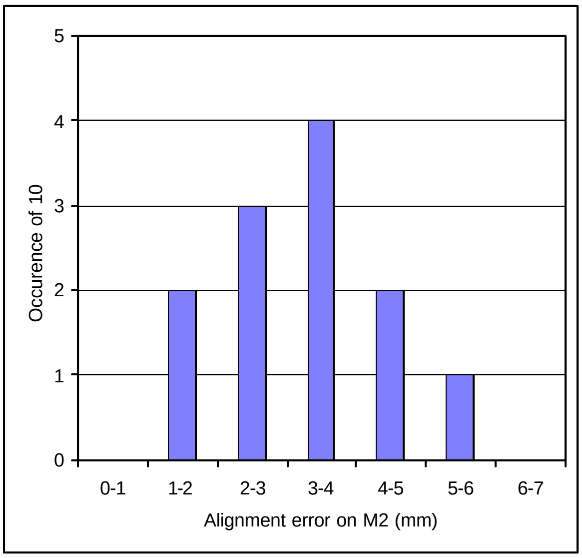

Figure 6. Monte Carlo analysis with 10 randomly generated combinations of alignment errors. Each mirror has been given decenters and tilts up to ±0.1mm and ±1arcmin in each direction with an even statistical distribution. The resulting average error is 3.4mm (DR/R = 2.2%) and the 90% percentile is at 4.8mm (DR/R = 3.2%), i.e. less than the RSS assumption made in the error budget (Figure 3). This provides a "confidence margin". [The RSS assumption actually works with standard deviations. Since the standard deviation of an even distribution between ±a is s = a/Ö3, there is a factor Ö3 between the Monte-Carlo average and the RSS sum: 2.2% Ö3 = 3.8%, compared with 4.0% in the budget.]

4. Spectrometer budgets

4.1. Throughput

In the spectrometer, an exactly-sized aperture stop (referred to as spectrometer cold stop, SCS) is located between SM6 and SM7 in connection with the passage of the beam through the optical bench. An image of this stop exists close to the detectors, between SM11A/B and SM12A/B, but this is not used due to mechanical constraints. Instead, the mirrors SM12A/B will be shaped according to the geometrical beam, playing the role of a partial stop avoiding detectors to see too far into the instrument. For the central detector, this stop will be oversized with respect to the SCS, for edge detectors it will be oversized on one side and exactly sized on the other side.

Similar alignment tolerances as those imposed on the photometer due to pupil alignment are imposed on the spectrometer due to interferogram contrast. A similar level of misalignment may therefore be expected between the two stops within the spectrometer as that calculated for internal alignment in the photometer. Since the stop on SM12A/B is not in a pupil image and sized as described above, the effect on throughput is smaller however and only seen for edge detectors. As a worst case, we have assumed the value given for internal alignment in the photometer budget, Sec. 3.3, ie. $\Delta R/R = 4\%$, hence $T = 1-0.64\ \Delta R/R = 97\%$.

Since the SCS is located early in the optical train, we assume the photometer value for external alignment ("Telescope to SPIRE interface" in Sec. 3.3) for its misalignment with the telescope pupil, ie. $\Delta R/R = 6\%$, hence $T = 1-0.64\ \Delta R/R = 96\%$.

Pupil aberrations due to the optical design are estimated to $\Delta R/R = 5\%$, hence $T = 1-0.64\ \Delta R/R = 97\%$.

Losses due to diffraction and baffling are estimated to 20% (TBC). We have assumed 99% reflectivity of each of 13 mirror surface (CM3 to SM12 plus three CC surfaces) and a total filter and beamsplitter efficiency of 40%.

The throughput loss of 50% due to band-pass filtering is not included (cf BMS).

Horn coupling efficiency is not accounted for, in accordance with IRD-OPTS-R05, neither on-axis or off-axis. The efficiency for edge detectors is particularly poor due to the telecentric horn arrangement.

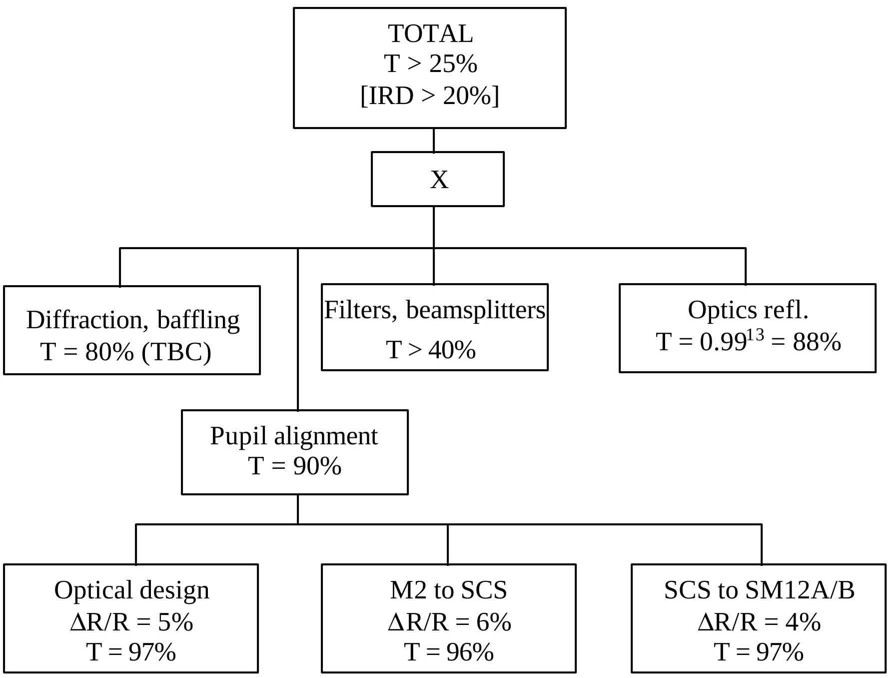

Figure 7. Spectrometer throughput budget.

4.2. Wavefront error

Wavefront error budget meets IRD. See Sec. 3.2 for comments.

RMS surface error of 1 µm (2µm WFErms) is assumed for each of 15 reflecting surfaces (CM3 to SM12 plus 3 CC surfaces plus 2 BS surfaces). Transmissive components are not included since their thickness is negligible.

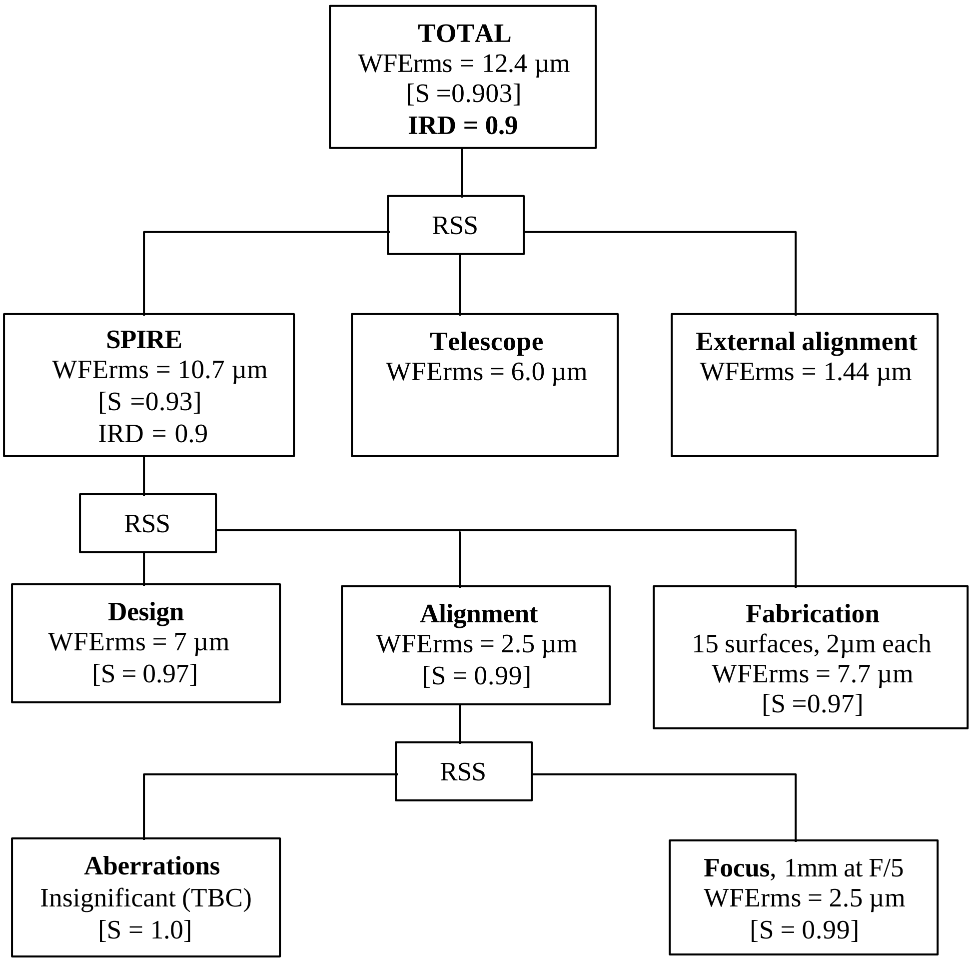

Figure 8. Spectrometer wavefront budget.

4.3. Interferogram contrast

Contrast is affected by tilt and shear between the interfering wavefronts and balance between beamsplitter R and T. Tilts and shears are discussed in the following, beamsplitter balance is discussed in sec. 4.3.5.

Interferogram contrast describes the efficiency with which the instrument renders the undulating interference intensity created by the FTS. It is defined for a monochromatic beam as:

$$k = \frac{I_{max} - I_{min}}{I_{max} + I_{min}} \tag{1}$$

where I_{max} and I_{min} are maximum (constructive) and minimum (destructive) interference intensities, respectively.

When OPD > 0, wavefronts from an off-axis object are sheared due to geometry, and may be tilted due to differential distortion. Misalignments of components within the interferometer also introduce tilt and shear.

4.3.1. Wavefront tilt

When interfering wavefronts are tilted in the pupil by angle q, the optical path difference varies across the pupil, i.e. Newtons fringes can be observed. This results in a reduced interferogram contrast which Lambert and Richards [RD2] calculated, for a uniformly illuminated circular pupil, using the van Cittert Zernike theorem:

$$k_T = 2J_1(u)/u \tag{2}$$

where $u = pqd/l$ and d is the diameter of the pupil. It is convenient to quantify the tilt in the pupil in terms of the resulting image shift at the detector: $D = qf$. Then: $u = pD/(lF)$. Applying the Taylor expansion to eq. (2) provides an approximation valid for small perturbations:

$$k_T \approx 1 - u^2/8 = 1 - 0.79\,\Delta^2 \tag{3a}$$

when l = 250µm and F = 5. For a Gaussian pupil function, clipped at 25% power level by a circular aperture defined by a focal ratio of F = 5, numerical calculations (figs 9 and 10) indicate a contrast function of:

$$k_T \approx 1 - 0.59\,\Delta^2 \tag{3b}$$

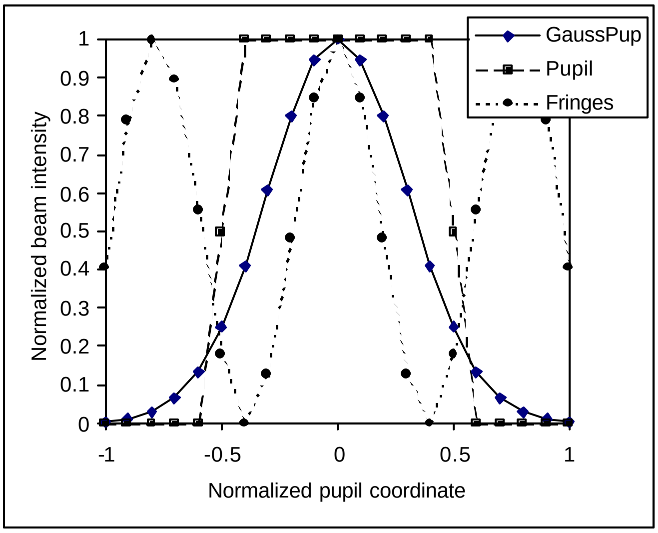

Figure 9. Beam patterns for calculation of wavefront tilt effect. Contrast is lost due to formation of Newton's fringes (dotted).

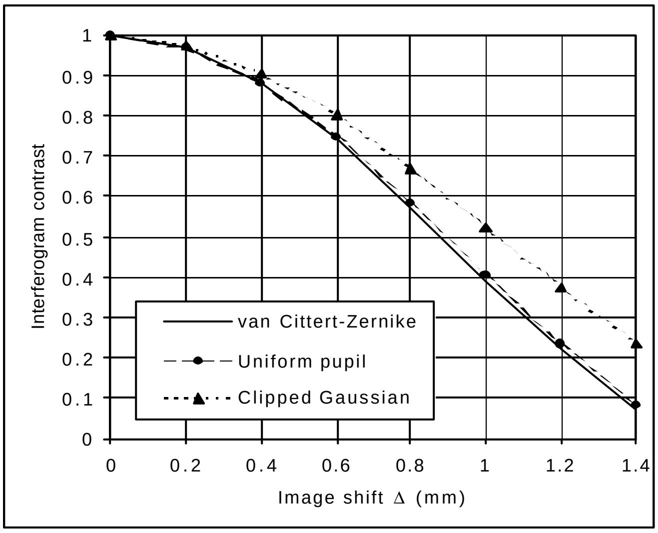

Figure 10. Comparison between contrast for uniform pupil and clipped-Gaussian pupil.

4.3.2. Wavefront shear

When the interfering wavefronts are sheared in the pupil, one must distinguish between coherent and incoherent radiation [RD2]. In the SPIRE case, where the objects under study are generally unresolved, hence coherent, the contrast function equals the MTF of the camera system. The MTF may be calculated as the autocorrelation of the complex pupil function. Assuming perfect optics, which is not far from being the case for SPIRE, the pupil function is real and equal to the pupil transmisison function. In the case of a uniform circular pupil, the contrast is therefore given by the classical diffraction limited MTF curve [RD4] and may be expressed as:

$$k_S = (2/\pi)[\mathrm{acos}(u) - u\sqrt{(1-u^2)}] \approx 1 - (4/\pi)u \qquad (4a)$$

when u is small, where $u = s/d$, s is pupil shear, and d is the pupil diameter. Note that this function falls off linearly with shear.

Numerical calculations shows that for a Gaussian pupil clipped at 25% power level by a circular aperture of diameter d (fig (11X), the fall-off is parabolic and approximately equal to (fig. 12):

$$k_S \text{ » } 1 - 3.3\, u^2 = 1 - 5.3 \times 10^{-3}\, s^2 \qquad (4b)$$

for a pupil of diameter d = 25 mm.

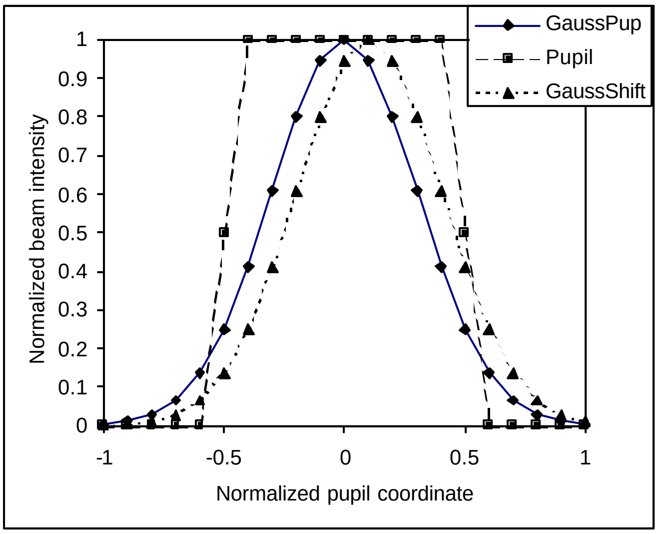

Figure 11. Beam patterns for calculation of wavefront shear effect.

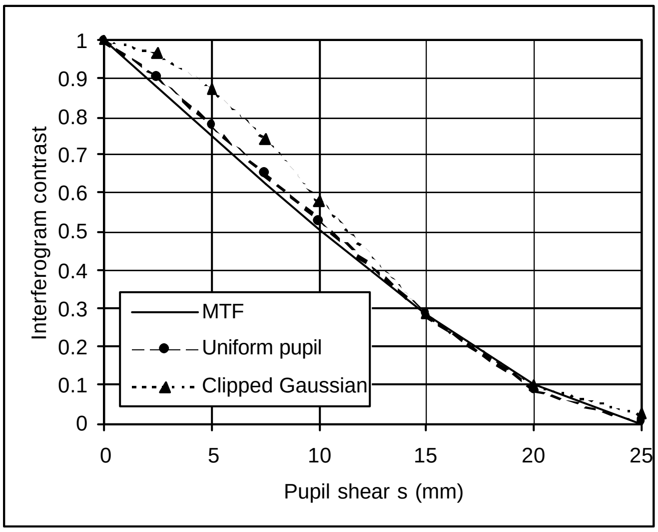

Figure 12. Comparison between contrast for uniform pupil and clipped-Gaussian pupil.

4.3.3. Optical design

Two sources of contrast loss due to optical design are identified:

1) Shear for off-axis object.

As seen in fig. 13, an off-axis beam travelling through the interferometer at angle β experiences a pupil shear of:

$$s = OPD \sin\beta \approx OPD\ \beta$$

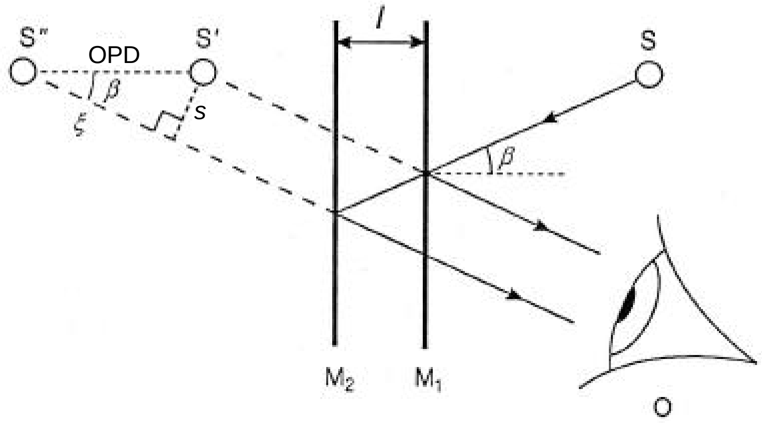

Figure 13. Shear for an off-axis beam in a two-beam interferometer.

The angle β for an object at the edge of the FOV is given by the Lagrange invariant as

$$\beta = FOV\ D/(2d)$$

where FOV is diameter of the sky field of view and D is the telescope entrance pupil diameter. Assuming FOV = 2.6′, D = 3300mm, d = 25mm, we get β = 2.86°. At the nominal resolving power of 100, the maximum OPD is 12.5mm, hence pupil shear is s = 0.62mm. At maximum resolving power (1000), the shear is s = 6.2mm. Contrasts estimated by eq (5) are 99.8% and 80%, respectively.

2) Tilt due to differential distortion.

Since there is powered optics within the interferometer and the OPD scanning causes a longitudinal displacement of the exit pupil, differential aberrations between the two interfering beams may occur. No significant difference in wavefront error has been detected, but a slight difference in distortion causes a shift of the image position (ie wavefront tilt) for off-axis objects. The shift increases linearly with OPD and reaches Δ = 0.04mm at R = 100 and Δ = 0.4mm at R = 1000. Contrasts estimated by eq. (3) are 99.9% and 90.6%, respectively.

The total theoretical contrast of the optical design is therefore 99.7% at R = 100 and 72.5% at R = 1000. This is to be compared with results obtained by ASAP analysis.

4.3.4. Interferometer alignment

Contrary to optical design losses, alignment losses are independent of OPD and FOV. Tilts and decenters of each component within the interferometer in general introduce both tilts and shears to the interfering wavefronts. Table 1 gives wavefront tilts and shears produced by 0.1mm decenters and 1′ tilts of each component within the interferometer. The RSS of tilt and decenter values are calculated, and the total budgets estimated by multiplication with √(2N), where the √2 factor accounts for errors in both x and y directions, and N is the number of components in each case. The total budgets shows fringe contrast in brackets.

Clearly, the most critical components are the collimator and camera mirrors. Any significant reduction in alignment precision of these components will have important impacts on the alignment budget. Beamsplitter and corner cube alignments are far less critical. Tolerances may be relaxed in these cases, this may be particularly interesting for the internal alignment of the corner cubes.

In discussions with Guy Michel and Don Jennings, it became clear that they considered some adjustment capability highly desirable, at least for the qualification model, to allow optimizing cold IR operation. CIRS was originally designed without adjustments, but this was included later and proved useful during “debugging” of the qualification model. It is not clear how this could be realised in SPIRE, but it should be discussed. Don also suggests that the imaging capability of SPIRE may be utilised in the cold alignment check, eliminating the need for "cold fiddeling". TBT (=To be thought about :)

Important note: The current budget concerns the scientific beam. Constraints due to mechanical or sensor concerns may in some cases be overriding.

Table 1. Wavefront tilts and shears due to 1¢ tilts and 0.1mm decenters

	1¢ tilt		0.1mm decenter		Total per comp, per dimension		Nb of units	Total budgets (contrast)	
Component	**Tilt, D (mm)**	**Shear, s (mm)**	**Tilt, D (mm)**	**Shear, s (mm)**	**Tilt, D (mm)**	**Shear, s (mm)**		**Tilt, D (mm)**	**Shear, s (mm)**
Beamsplitter	0.023	0.087	0	0	0.023	0.087	2	0.046 (99.9%)	0.174 (99.98%)
Collimator	0.075	0.087	0.1	0.12	0.13	0.15	2	0.26 (96%)	0.30 (99.95%)
Camera	0.075	0.087	0.1	0.12	0.13	0.15	2	0.26 (96%)	0.30 (99.95%)
CC relative[1]	0	0	0	0.2	0	0.2	2	0 (100%)	0.40 (99.92%)
CC internal[2]	0.038	0	NA	NA	0.038	0	2	0.076 (99.7%)	0 (100%)
CC scan axis[3]	0	0	0	0	0	0	1	0 (100%)	0 (100%)
Total								**91.6%**	

Notes:

1) Relative alignment between upper and lower CC vertices. Axial separation is not critical for contrast but should be kept below 1 mm.

2) Misalignments of the CC facets which cause 1′ beam deviation between input and output beams is assumed.

3) Fringe contrast is insensitive to tilts and decenters of perfectly mounted back-to-back corner cubes during the scan. Decenters give pupil movement however, so to avoid vignetting, the decenter should be less than 1 mm, say.

4.3.5. Beamsplitter balance

If interference is formed between two wavefronts of intensity I_1 and I_2, then the contrast of the interference fringes may be expressed as:

$$k = \frac{2\sqrt{I_1 I_2}}{I_1 + I_2} . \qquad (6)$$

In a Mach-Zehnder, dual output configuration with two identical beamsplitters of reflectivity R and transmissivity T, the intensities I_1 and I_2 may be expressed in terms of R and T for each of the two outputs A and B:

$$I_{1A} = I_{2A} = RT, \qquad (7)$$

$$I_{1B} = R^2 \quad \text{and} \quad I_{2B} = T^2. \qquad (8)$$

By eq. (6) we therefore have:

$$k_A = 1,$$

$$k_B = 2RT/(R^2 + T^2).$$

The A output therefore has 100% contrast regardless of beamsplitter performance. Reading values of R and T off the curves presented by PA at the July 99 PDR [RD3], we find approximate contrast values for the B output, see Table 2. For the budget we have taken the worst-case contrast of 94%, occuring at 190 and 500 µm.

Table 2. Approximate contrast for the B output.

λ (µm)	**R (%)**	**T (%)**	**k_B (%)**
190	58	40	93.5
250	51.5	46	99.4
333	54.3	43.9	97.7
500	56	40	94.6
625	46	46	100
1000	26	67	67.5

4.3.6. Budget

Figure 14 shows the interferometer alignment budget. Nominal (R = 100) contrast values are shown and R = 1000 values are indicated in brackets. With a total budget of 85.8% for nominal resolving power, the required contrast of 80% is achieved with margin.

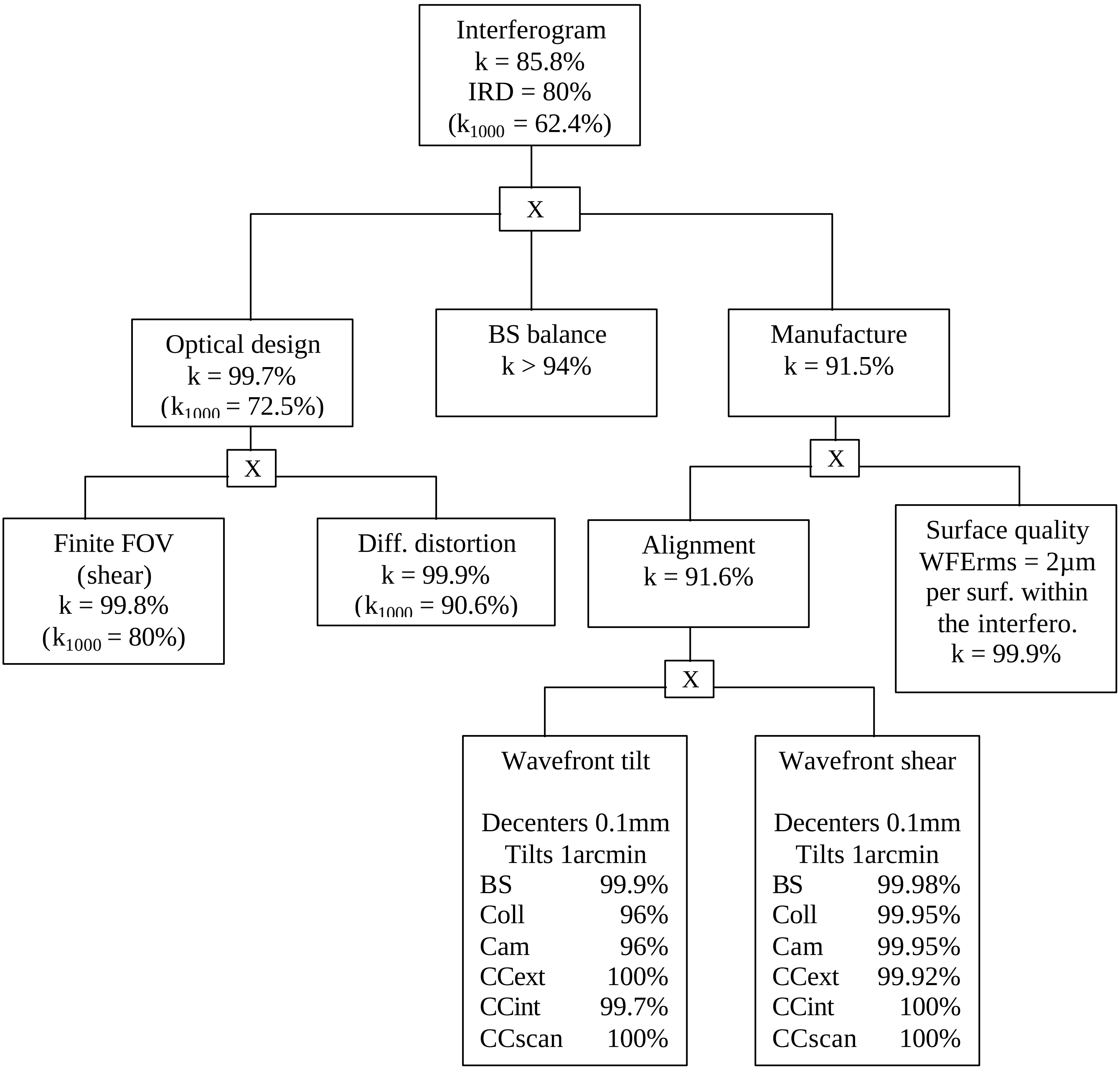

Figure 14. Interferometer alignment budget calculated at 250 µm. Nominal (R = 100) contrast values are shown and R = 1000 values are indicated in brackets.